Society for Integrative and Comparative Biology

### **SYMPOSIUM**

### Body stiffness and damping depend sensitively on the timing of muscle activation in lampreys

Eric D. Tytell,<sup>1,\*</sup> Jennifer A. Carr,<sup>2,\*</sup> Nicole Danos,<sup>3,\*</sup> Christopher Wagenbach,<sup>\*</sup> Caitlin M. Sullivan,<sup>†</sup> Tim Kiemel,<sup>‡</sup> Noah J. Cowan<sup>§</sup> and M. Mert Ankarali<sup>¶</sup>

\*Department of Biology, Tufts University, Medford, MA 02155, USA; †Department of Biology, Emmanuel College, Boston, MA 02115, USA; <sup>‡</sup>Department of Kinesiology, University of Maryland, College Park, MD 20742, USA; Department of Mechanical Engineering, Johns Hopkins University, Baltimore, MD 21218, USA; Department of Electrical and Electronics Engineering, Middle East Technical University, Ankara, Turkey

From the symposium "Sensory Feedback and Animal Locomotion: Perspectives from Biology and Biorobotics" presented at the annual meeting of the Society for Integrative and Comparative Biology, January 3-7, 2018 at San Francisco, California.

<sup>1</sup>E-mail: eric.tytell@tufts.edu

<sup>2</sup>Present address: Department of Biology, Salem State University, Salem, MA 01970, USA

<sup>3</sup>Present address: Department of Biology, University of San Diego, San Diego, CA 92110, USA

Synopsis Unlike most manmade machines, animals move through their world using flexible bodies and appendages, which bend due to internal muscle and body forces, and also due to forces from the environment. Fishes in particular must cope with fluid dynamic forces that not only resist their overall swimming movements but also may have unsteady flow patterns, vortices, and turbulence, many of which occur more rapidly than what the nervous system can process. Has natural selection led to mechanical properties of fish bodies and their component tissues that can respond very quickly to environmental perturbations? Here, we focus on the mechanical properties of isolated muscle tissue and of the entire intact body in the silver lamprey, Ichthyomyzon unicuspis. We developed two modified work loop protocols to determine the effect of small perturbations on the whole body and on isolated segments of muscle as a function of muscle activation and phase within the swimming cycle. First, we examined how the mechanical properties of the whole lamprey body change depending on the timing of muscle activity. Relative to passive muscle, muscle activation can modulate the effective stiffness by about two-fold and modulate the effective damping by >10-fold depending on the activation phase. Next, we performed a standard work loop test on small sections of axial musculature while adding lowamplitude sinusoidal perturbations at specific frequencies. We modeled the data using a new system identification technique based on time-periodic system analysis and harmonic transfer functions (HTFs) and used the resulting models to predict muscle function under novel conditions. We found that the effective stiffness and damping of muscle varies during the swimming cycle, and that the timing of activation can alter both the magnitude and timing of peak stiffness and damping. Moreover, the response of the isolated muscle was highly nonlinear and length dependent, but the body's response was much more linear. We applied the resulting HTFs from our experiments to explore the effect of pairs of antagonistic muscles. The results suggest that when muscles work against each other as antagonists, the combined system has weaker nonlinearities than either muscle segment alone. Together, these results begin to provide an integrative understanding of how activation timing can tune the mechanical response properties of muscles, enabling fish to swim effectively in their complex and unpredictable environment.

#### Introduction

As an animal moves through its environment, unexpected forces will cause the animal's body and appendages to deform and respond mechanically, even before the nervous system has time to sense the effect and respond (Brown and Loeb 2000; Jindrich and Full 2002). For fishes, these forces often come from the complex and unpredictable fluid flow

patterns that occur naturally in rivers, waves, or in nearly any water flow (Lacey et al. 2012). The bodies of fishes are composed of muscle, cartilage, bones, tendon, skin, and other complicated mechanical elements, all linked together in an intricate three-dimensional structure, often with nonlinear mechanical properties (Summers and Long 2005), making them particularly well suited for investigating the interplay between passive body dynamics and feedback control (Tytell et al. 2011; Roth et al. 2014). When a fish swims, the body bends back and forth, partially due to the internal muscular forces and partially due to the external fluid dynamic forces. As it cycles through this pattern, the body will also respond to any unexpected forces due to vortices or turbulent flow patterns. Thus, understanding how fish bodies respond mechanically to perturbations is crucial for understanding how they navigate their complicated and unpredictable environment.

We know that the nervous system responds differently depending on when a perturbation occurs. This effect is well known in walking animals, like cats or humans: if a cat's foot strikes an obstacle just as it is beginning a step, it will lift its foot up and over the obstacle, but if it strikes the obstacle toward the end of a step, it will just put the foot down (Forssberg et al. 1975; Rossignol et al. 2006). Similarly, in lampreys, neural circuits in the spinal cord respond differently to perturbations at different phases within the swimming cycle (Massarelli et al. 2016).

The body may respond to perturbations differently at different times (Brown and Loeb 2000; Jindrich and Full 2002; Holmes et al. 2006; Proctor and Holmes 2010). For example, many body tissues have nonlinear responses, meaning that they change stiffness at high strain compared to low strain (Danos and Azizi 2015; Porter et al. 2016). Similarly, damping, or viscosity, may change with strain or strain rate (Long et al. 2002). Furthermore, the properties of muscle depend on its activation. Muscle is stiffer when it is lengthened while active than when it is shortening while active (Ettema and Huijing 1994a; Monroy et al. 2017), and has higher damping at large strain than at small strain (Lin and Rymer 2000). Even the aponeuroses around the muscle can change their effective properties when the muscle is active (Azizi and Roberts 2009). In cockroaches, the timing of muscle activation relative to movement phase can make two anatomical extensors in the same joint act like a motor or a brake (Ahn and Full 2002; Sponberg et al. 2011).

Here we use two different sets of techniques to assess the mechanical properties of the whole body of lampreys and of isolated muscle segments. We use large amplitude oscillatory bending theory (after Porter et al. 2016) to quantify how the body properties change with muscle activation. We then quantify the properties of isolated muscle segments using harmonic transfer functions (HTFs) (Wereley 1991; Sandberg et al. 2005; Kiemel et al. 2016), an extension of classic time-invariant transfer functions (Ogata 2010) that allow us to quantify the response of muscle to perturbations as a function of phase.

Lampreys are a well-established model system for understanding the neural control of locomotion (Grillner 2003; Tytell et al. 2011). In particular, they are the only vertebrate for which we know the cells and their connectivity that make up the central pattern generator, the neural circuit that generates locomotion (Grillner et al. 1991; Parker 2006), and the only non-tetrapod vertebrate for which we know the proprioceptive sensory cells that allow the animal to sense its own movement (Grillner et al. 1984; Massarelli et al. 2017). Adult lampreys are active migratory fishes, capable of high speed swimming (Mesa et al. 2003; Dauble et al. 2006), though they are not quite as athletic as some teleost fishes (Quintella et al. 2004). They swim in typically an anguilliform mode, with a traveling wave of curvature that moves down the body (Fig. 1). Axial muscles tend to become active before shortening (Fig. 1A), with more activity during lengthening close to the tail (Fig. 1B) (Williams et al. 1989). Unlike teleost fishes, lampreys have mixed red and white muscle in their axial musculature (Teräväinen 1971; Kimura et al. 1995), a condition more similar to tetrapods than more derived fishes. To integrate these results with what is known about swimming biomechanics, we need to understand the structure and mechanics of the lamprey's muscle and body.

Below, we briefly introduce the theory behind the two techniques used in this study, and then describe the results of these tests on the mechanics of lamprey bodies and muscle.

### Whole-body bending mechanics

We quantified the bending mechanics of lamprey body using the nonlinear large amplitude oscillatory bending technique (Ewoldt et al. 2008; Porter et al. 2016). Briefly, we bent the body with a sinusoidal curvature,  $\kappa = \kappa_0 \sin \omega t$ , where  $\kappa$  is curvature (0 is straight; positive values indicate bending concave to the animal's right),  $\kappa_0$  is the bending amplitude, and  $\omega$  is the bending frequency. For a linear material, the torque  $\tau$  can be represented with a constant elastic and damping moduli EI and  $\eta I$ 

$$\tau = \kappa_0(EI\sin\omega t + \eta I \ \omega\cos\omega t).$$

For nonlinear materials, EI and  $\eta I$  will vary depending on curvature or curvature rate. Following Porter et al. (2016), we estimate three coefficients:  $E_1I$ , the average modulus;  $E_MI$ , the

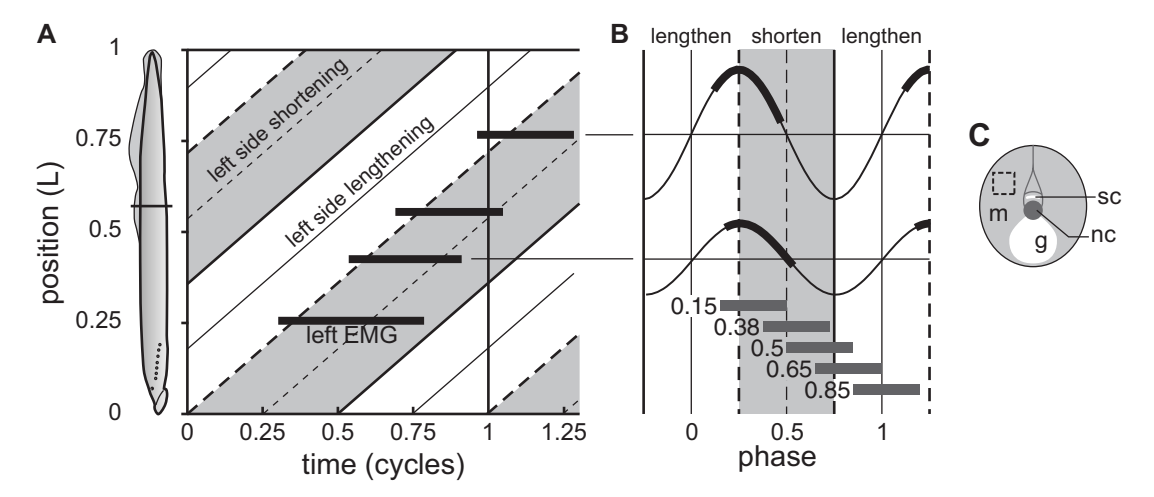


Fig. 1 Schematic of muscle activity and anatomy during swimming in lampreys. (A) Timing of curvature and muscle activity during free swimming in lampreys. Gray bars represent when the muscle on the left side of the animal is shortening, and solid lines show the timing of muscle electromyograms (EMG). Modified from Tytell and Cohen (2008). EMG data from Williams et al. (1989). (B) Phase of muscle activity relative to curvature for the second and fourth channels from A, where thick black lines represent muscle activity. The labeled bars show the phases of isolated muscle stimulation. (C) Cross-sectional anatomy of a lamprey at 55% of body length. The dashed square shows the approximate location of isolated muscle samples. m, muscle; g, gut cavity; nc, notochord; sc, spinal cord.

modulus at zero curvature; and  $E_L I$ , the modulus at the largest curvature

$$E_{M}I = \frac{d\tau}{d\kappa} \Big|_{\kappa=0, \ \kappa=\omega\kappa_{0}} \qquad ELI = \frac{\tau}{\kappa} \Big|_{\kappa=\kappa_{0}, \ \kappa=0}$$
 (1)

and similarly,  $\eta_1 I$ ,  $\eta_M I$ , and  $\eta_L I$ ,

$$\eta_M I = \frac{d\tau}{d\dot{\kappa}} \Big|_{\dot{\kappa} = 0, \ \kappa = \kappa_0} \qquad \eta L I = \frac{\tau}{\dot{\kappa}} \Big|_{\dot{\kappa} = \omega \kappa_0, \ \kappa = 0}$$
 (2)

where  $\dot{\kappa}$  is the rate of change of curvature. All metrics assume that the torque response is symmetric for bending to opposite sides (Ewoldt et al. 2008). For a material that responds linearly with respect to curvature, all three EI and  $\eta I$  parameters are equal.

## HTF approach for isolated muscle mechanics

The analysis of HTFs makes it straightforward to estimate the phase-dependent properties of a system. To illustrate this approach to data analysis and modeling, consider a simple system that has a phase dependent stiffness  $k(\phi) = k_1 \cos(\phi - \delta)$ , where  $k_1$  is the maximum stiffness,  $\delta$  is the phase of maximum stiffness, and  $\phi$  is the phase of the system. In this simple example, the "stiffness" can be negative. Then the force that the system produces is

$$F = k(\phi)x,\tag{3}$$

where x is the displacement relative to its baseline length and  $\phi = \omega t$ , where  $\omega$  is the fundamental frequency of the system.

If we perturb the system at a frequency  $\alpha$  different from the fundamental frequency  $\omega$  then the output force will oscillate not only at frequency  $\omega$  and  $\alpha$ , but at  $\omega + \alpha$  and  $\omega - \alpha$ . We can see this effect using the trigonometric identity  $\cos \theta$   $\cos \phi = \frac{1}{2} \cos (\theta - \phi) + \frac{1}{2} \cos (\theta + \phi)$ . Substituting  $x = A_1 \cos \alpha t$  into Equation (3) yields

$$F = \frac{1}{2}k_1A_1 \begin{bmatrix} (\cos \delta + \sin \delta)\cos([\alpha - \omega]t) \\ + (\cos \delta - \sin \delta)\cos([\alpha + \omega]t) \end{bmatrix}.$$

Using the Fourier transform, we can isolate the output amplitudes of the system at frequency  $\alpha + \omega$  and  $\alpha - \omega$  and use them to estimate  $k_1$  and  $\delta$ .

Now, consider the phase dependent stiffness and damping of muscle. We impose a baseline oscillation in strain  $x^*$  and activation that produces the baseline stress  $F^*$ , add on small perturbations, and measure their effect on the force

$$F_d = k(\phi)x_d + b(\phi)\frac{\partial x_d}{\partial t},$$

where  $F_d = F - F^*$ ,  $x_d = x - x^*$ , and  $k(\phi)$  and  $b(\phi)$  are the stiffness and damping, respectively.

To account for the complexity of the muscle's response, the stiffness and damping functions may be more complicated than a pure cosine. They must be periodic, which means we can write them as Fourier series, that is, sums of sines and cosines at frequencies  $\omega$ ,  $2\omega$ ,  $3\omega$ ,...,  $p\omega$ . In terms of complex

exponentials,  $k = \sum_{p \in \mathbb{Z}} k_p e^{ip\omega t}$  and  $b = \sum_{p \in \mathbb{Z}} b_p e^{ip\omega t}$ , where  $\mathbb{Z}$  is the set of all integers. To ensure that the values are real,  $k_{\pm p} = \frac{1}{2} \left( k_p^c \mp i k_p^s \right)$  and  $b_{\pm p} = \frac{1}{2} \left( b_p^c \mp i b_p^s \right)$  for  $p \neq 0$ , where  $k_p^c$ ,  $k_p^s$ ,  $b_p^c$ , and  $b_p^s$  are the real coefficients of cosine and sine terms, respectively. Multiple perturbation frequencies can be applied at the same time, so that  $x_d = \sum_{j=-N}^N a_j e^{i\alpha_j t}$ , where  $a_0 = 0$  and  $\alpha_j = -\alpha_{-j}$ .

After a tedious but straightforward derivation, we find that

$$F = \sum_{j=-N}^{N} \sum_{p \in \mathbb{Z}} a_j (k_p + i\alpha_j b_p) e^{i(\alpha_j + p\omega)t}$$

The HTF  $H_p(\alpha_j)$  comprises the set of ratios of the output at frequency  $\alpha_j + p\omega$  divided by the input at frequency  $\alpha_j$ , or

$$H_p(\alpha_j) = k_p + i\alpha_j b_p$$

Since the perturbations and output must be real, we can estimate the real coefficients of stiffness and damping in terms of the real and imaginary components of the HTF

$$k_{p}^{c} = Re\{H_{p}(\alpha_{j})\} + Re\{H_{-p}(\alpha_{j})\}$$

$$k_{p}^{s} = -Im\{H_{p}(\alpha_{j})\} + Im\{H_{-p}(\alpha_{j})\}$$

$$b_{p}^{c} = \frac{1}{\alpha_{j}}[Im\{H_{p}(\alpha_{j})\} + Im\{H_{-p}(\alpha_{j})\}]$$

$$b_{p}^{s} = \frac{1}{\alpha_{j}}[Re\{H_{p}(\alpha_{j})\} - Re\{H_{-p}(\alpha_{j})\}].$$

$$(4)$$

In principle, for each perturbation frequency  $\alpha_j$ , we can use the equations above to estimate all of the  $H_p$  modes, giving us an estimate of both stiffness and damping. In practice, the stiffness is most evident at low frequencies and damping at high frequencies, but the breakpoint between "low" and "high" depends on the relative magnitude of the stiffness and damping.

#### **Methods**

### Animals and preparations

Silver lampreys *Ichthyomyzon unicuspis* were purchased from a commercial supplier (Ritter's Fish Market, Prarie du Chien, WI) and housed together in a 220 gal tank at 4°C and a 12:12 hr light:dark cycle. To isolate the muscle or the body, an animal was anesthetized in a solution of ethyl 3-aminobenzoate methanesulfonate (MS222; 0.2 g/L; Sigma Aldrich, St. Louis,

MO), buffered to pH 7.4. The animal was than euthanized by rapid decapitation and pithing the brain. The tail was removed by cutting the body at the anus. The body was placed in a tray containing cold physiological saline (NaCl, 124 mM; KCl, 0.5 mM; CaCl<sub>2</sub>, 1.1 mM; MgCl<sub>2</sub>, 0.5 mM; glucose, 5.5 mM; NaHCO<sub>3</sub>, 10.0 mM) (Cameron and Tufts 1994). All animal procedures were approved by the Tufts University Institutional Animal Care and Use Committee (protocol numbers M2012-145 and M2015-149).

### Estimation of whole body parameters

For whole body tests, we cut a body segment,  $\sim 10 \text{ cm}$ long, centered 55% of the distance from head to tail (Fig. 1C). The rostral end was clamped to a force transducer (Mini-40, ATI Industrial Automation, Apex, NC) and the caudal end was clamped to a servomotor (SDK-2310S-ELN, Teknic, Victor, NY). Figure 2A shows a schematic of the setup. Platinum stimulating electrodes (Natus Manufacturing F-E2) were implanted, one pair each on the left and right side, and connected to stimulators (Model 2200, A-M systems, Sequim, WA). Stimuli were delivered as pulse trains with 1 ms pulses at 75 Hz for 30% of the cycle, with the left side 50% out of phase with the right. A custom Python program was used to record data and control the motor and the stimulator, using a data acquisition system (PCI-6221, National Instruments, Austin, TX).

The body was bent back and forth for 14 cycles (3 initial passive cycles, 10 cycles for analysis, and 1 final cycle) at an amplitude of either 2.5° or 5° and the resulting torques recorded. The true motor position was recorded using an encoder. The torque on the body  $(\tau_{\text{body}})$  was estimated based on the torque around the z axis  $(\tau_z)$  of the force transducer as  $\tau_{\text{body}} = \tau_z d_{\text{in}}/d_{\text{out,vert}}$  (Fig. 2A), where  $d_{\text{in}}$ is the horizontal distance between the center of the experimental segment and the center of the rostral clamp and  $d_{\text{out,vert}}$  is the vertical distance between the center of the clamp and the center of the transducer. Curvature  $\kappa$  was estimated as  $\theta/d_{\text{clamp}}$ , where  $\theta$  is the angle of the motor in radians and  $d_{clamp}$  is the distance between the clamps. The mean bending modulus  $E_1I$  is the axis that runs through the center of the  $(\kappa, \tau_{\text{body}})$  curve, and the mean damping modulus  $\eta_1 I$  is the axis of the  $(\kappa, \tau_{\text{body}})$  curve; both were estimated using a reduced major axis regression (Matlab's PCA function). We directly estimated  $E_M I$ ,  $E_L I$ ,  $\eta_M I$ , and  $\eta_L I$  by evaluating the appropriate points on the curve (Equations (1) and (2)).

We also estimated the whole-body work by integrating torque relative to curvature over the entire

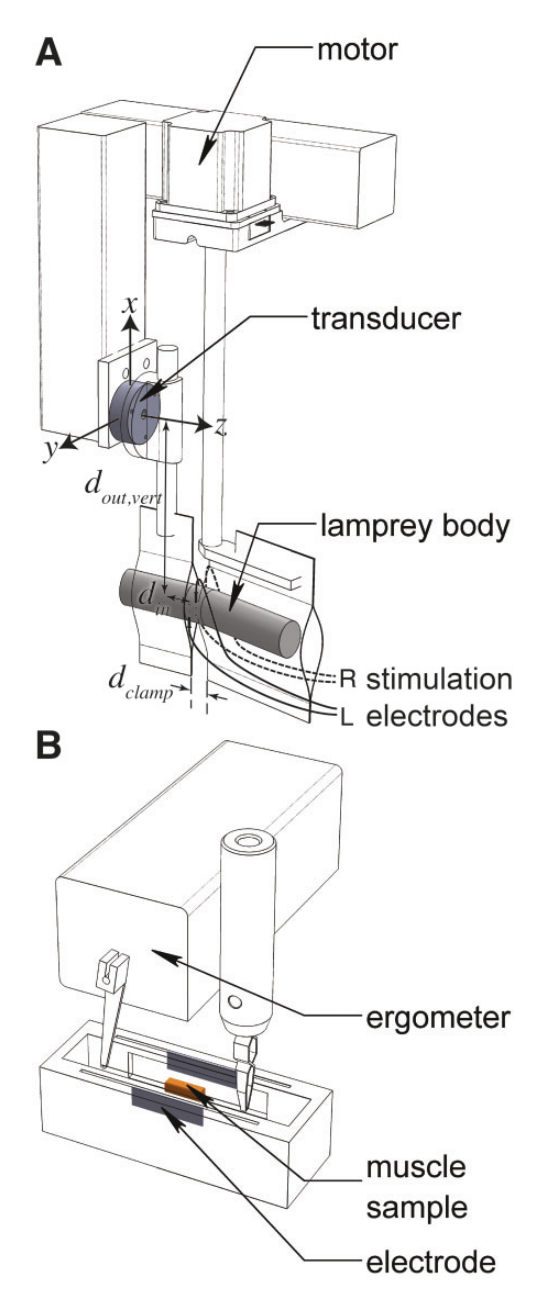


Fig. 2 Schematics of the mechanical testing setups. (A) Whole body setup. (B) Isolated muscle setup.

cycle,  $W = \int \tau_{\text{body}} d\kappa$ . We have defined the signs of  $\tau_{\text{body}}$  and  $\kappa$  so that a counter-clockwise work loop corresponds to positive net muscle mechanical work.

### Isolated muscle segments

For isolated muscle segments, the body was skinned and segments of muscle were dissected from the body wall while it was submerged in cold, aerated saline. Figure 1C shows the approximate size and location of the muscle segments. Individual muscle segments were secured using Kevlar thread between a

fixed attachment site and an ergometer arm so that two intact myomeres were between the Kevlar knots in the apparatus (Fig. 2B). During the experiment, muscle segments were secured in a recirculating saline bath kept at 10°C. We stimulated the muscle with two platinum plate electrodes using 80 V pulses at 35 pulses per second for 35% of the cycle. A custom Igor Pro (WaveMetrics, Lake Oswego, OR) program was used to record data and control the ergometer and the stimulator using a data acquisition system (National Instruments USB-6216, Austin, TX).

We first measured a muscle length–tension curve using twitch stimuli. Length–tension curves were measured regularly during the experiment to ensure that the muscle was not fatiguing too rapidly or slipping out of the knots. Experiments were ended in the rare case that the optimal force dropped to less than 85% of the initial value (following Peplowski and Marsh 1997) indicating that the muscle was fatiguing.

During the work loop experiments, we tested muscle segments with and without stimulation and with and without perturbations. We started each trial at a length where the force produced was 85% of the optimal force from the length-tension curves. During unperturbed trials the muscle segment cycled through sinusoidal length changes of 6% of resting length at frequency of 1 Hz. Perturbed trials were done at the same baseline amplitude and frequency, adding on 11 or 15 sinusoidal perturbation signals with frequencies between 0.3 and 75.1 Hz, chosen so that they did not overlap harmonics of the fundamental oscillation and so that their sums and differences did not overlap (following the procedure in Ankarali and Cowan 2014). The maximum perturbation amplitude was 8% of the baseline amplitude, and we reduced the amplitude at higher frequencies proportional to  $\alpha^{0.5}$  so that perturbation velocities did not become too large. Four phases of activation were used, with stimulation beginning at a phase of 0.15, 0.38, 0.65, or 0.85.

We estimated the muscle work by integrating stress relative to strain,  $W = -\int F \, dx$ , over the entire lengthening and shortening cycle. Net positive work is thus done when the magnitude of the work done by the muscle during shortening is larger than the magnitude of the work done on the muscle during lengthening.

### **Estimation of HTFs**

The HTF  $H_p(\alpha)$  is the output amplitude at a frequency  $\alpha + p\omega$  divided by the input amplitude at frequency  $\alpha$ .

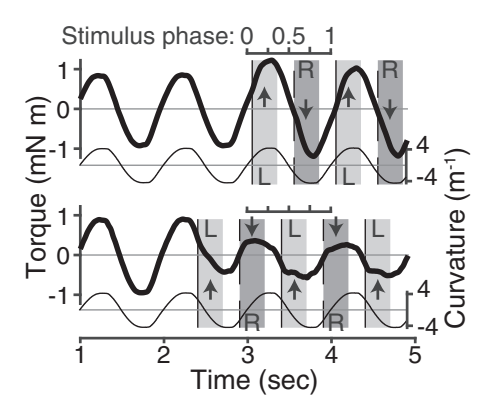


**Fig. 3** Example recordings from the whole body setup. Stimulation is shown with gray bars, labeled 'L' or 'R' for left or right side stimulation, respectively, with arrows to indicate the direction of muscle torque on that side. Stimulation phase is shown above, defined relative to the left side stimulation.

To calculate these quantities, we directly evaluated the complex Fourier integrals,  $X(\alpha) = \int x(t) e^{2\pi i \alpha t} dt$  and  $F(\alpha + p\omega) = \int f(t) e^{2\pi i (\alpha + p\omega)t} dt$  so that

$$H_p(\alpha) = \frac{\langle F(\alpha + p\omega)F^*(\alpha + p\omega)\rangle}{\langle X(\alpha)X^*(\alpha)\rangle}$$

where x(t) is the strain, f(t) is the stress,  $\langle \cdot \rangle$  denotes a mean, and  $F^*$  denotes the complex conjugate of F. We averaged three intervals with a 50% overlap spanning the time when perturbations were applied. Stiffness and damping were estimated from the HTFs according to Equation (4). We also estimated the stiffness at maximum length and at mean length for both single muscles and pairs of antagonists.

To estimate the effect of a pair of antagonistic muscles, we shifted one transfer function by  $180^{\circ}$  and then added it to the original. Shifting the phase requires multiplying by  $e^{ip\delta}$ , where  $\delta$  is the phase offset and p is the order of the HTF, so that the transfer function for the pair of antagonists is  $H_p^{\rm ant}(\alpha) = H_p(\alpha) + H_p(\alpha)e^{ip\pi} = H_p(\alpha) + (-1)^p H_p(\alpha)$ , which means doubling the even modes and cancelling out the odd ones.

### Results

### Whole body mechanics

We measured the body torque as a function of curvature and muscle activation phase. Figure 3 shows examples of the raw recordings at two stimulation phases (0.041 and 0.390), and Fig. 4A shows example of the resulting whole body work loops from the same individual. For all procedures, phase was defined relative to the center position, so that muscle shortening started at a phase of 0.25 and ended at 0.75, and the stimulation duration was always 30%

of a cycle, enabling us to isolate the effect of muscle activation timing on mechanical response properties.

We collected data from five silver lampreys *I. uni-cuspis*, of total length  $260 \pm 33$  mm (mean  $\pm$  standard deviation). The mechanical testing was centered on 55% of the body length, where animals had a mean cross section width of  $13.6 \pm 1.9$  mm and height of  $24.3 \pm 4.3$  mm, corresponding to a second moment of area *I* of  $3300 \pm 1700$  mm<sup>4</sup>.

The body produced net positive mechanical work when the muscles were activated at a starting phase as early as 0.95 up until shortly after the beginning of shortening (Fig. 4B). The largest net negative work was produced when the muscles started activation at a phase between 0.55 and 0.75, ending between 0.85 and 1.05.

We estimated three stiffness parameters:  $E_1I$ , the mean overall bending modulus;  $E_MI$ , the bending modulus at maximum curvature; and  $E_LI$ , the bending modulus at low curvature (Equations (1) and (2)) (Porter et al. 2016). We then estimated the equivalent material properties,  $E_1$ ,  $E_M$ , and  $E_L$ , by dividing by the second moment of area I. The passive stiffness  $E_1$  of the lamprey body for five preparations is shown in Fig. 4C and varies more than two-fold among animals.

### Effective body mechanics depends on muscle activation phase

When muscles are active, stiffness can be nearly double or less than half the passive stiffness, depending on the activation phase. The effective stiffness is greatest  $(1.57\pm0.3 \text{ times passive})$  when muscle begins activation at the beginning of lengthening (phase 0.76), although the largest net negative work is produced when the muscle begins activity earlier. Similarly, the effective stiffness is lowest  $(0.45\pm0.3 \text{ times passive})$  when the muscle begins activation at the beginning of shortening (phase 0.38), but the largest net positive work is produced when muscle activation starts before shortening.

Although stiffness changes with activation phase, a nonlinear property, the stiffness is fairly linear with curvature (Fig. 4D). The stiffness at minimum curvature is usually close to the stiffness at large curvature (Fig. 4C). For most phases,  $E_L/E_M$ , an index of nonlinear elastic material properties (Porter et al. 2016), ranges between 0.65 and 2.8. At phase 0.4,  $E_M$ , the stiffness at zero curvature, is small and highly variable across preparations (Fig. 4C), which means that some preparations are much more nonlinear at this phase than others, with one preparation reaching a nonlinearity of 7.9.

Active body damping can be substantially larger or smaller than passive damping, depending on the

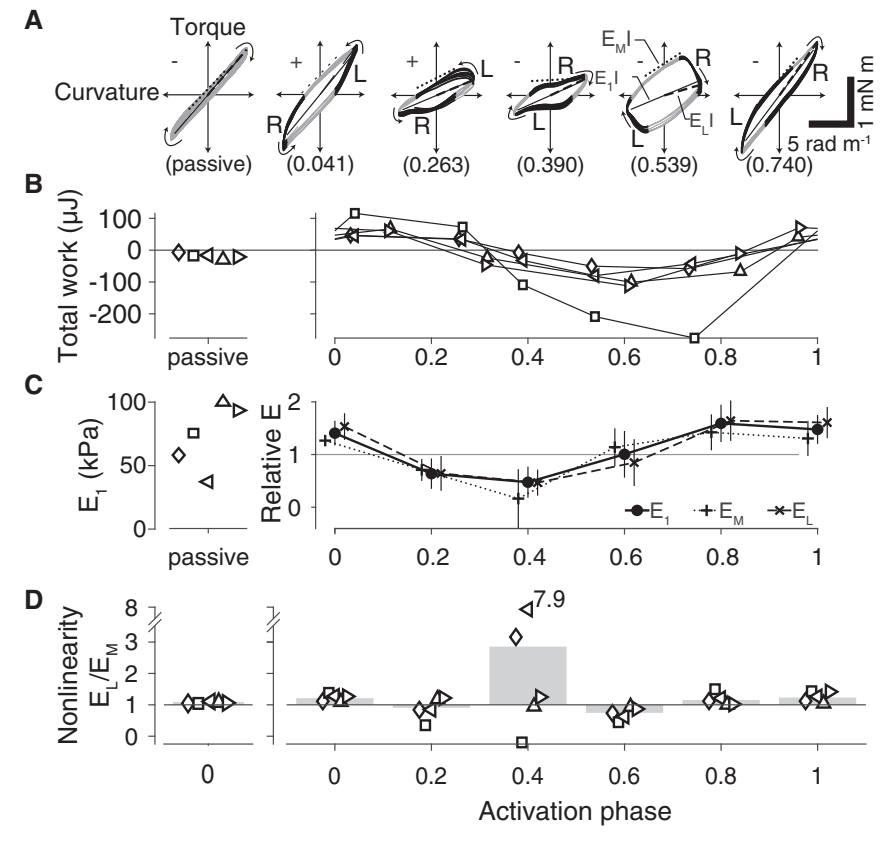


Fig. 4 Effective body stiffness varies depending on muscle activation phase. (A) Whole body work loops for a segment of lamprey body, showing the torque used to bend the body against curvature. Dark lines on the loop indicate the time of muscle stimulation at the phase shown in parentheses below each loop. 'R' and 'L' indicate whether the stimulation is on the right or the left. Small arrows show the direction of time in the loop and a '+' or a '-' sign indicates net positive or net negative mechanical work. The three bending moduli are indicated on each curve ( $E_1l$ , the mean overall modulus, solid line;  $E_Ml$ , the modulus at maximum curvature, dashed line; and  $E_Ll$ , the modulus at zero curvature, dashed line, displaced upward for clarity). (B) Total work done by the muscle. Different symbols indicate different individual preparations. (C) Overall mean stiffnesses  $E_1$ ,  $E_M$ , and  $E_L$ , relative to the passive  $E_1$  stiffness. Error bars represent standard deviation and points have been jittered to avoid overlap. (D) Nonlinearity  $E_L/E_M$ . Means are shown as shaded bars relative to 1, which represents a linear response, and points are individual preparations.

timing of activation, and is always nonlinear (Fig. 5). In particular, the damping  $\eta_M$  at zero curvature rate can be as much as 22 times larger or -13 times smaller than passive damping. Mean damping  $\eta_1$  is highest  $(6.9\pm4$  times passive) when muscle is activated starting at phase 0.55 and lowest  $(-4\pm2$  times passive) at phase 0. Figure 5C shows the viscous nonlinearity parameter  $\eta_L/\eta_M$ . Unlike stiffness, damping is always nonlinear; the damping at large curvature rates  $(\eta_L)$  is always substantially lower than the damping at zero curvature rate  $(\eta_M)$ . When the body is producing net positive mechanical work, the damping parameters are negative, indicating that it takes less torque to move faster.

#### Mechanical properties of isolated muscle segments

We used a standard work loop procedure to quantify the work done by muscle segments as a function of activation phase (Fig. 6). Muscle produces positive work when activated shortly before lengthening, at a phase of 0.15, the phase normally used during steady swimming at this location on the body (Fig. 1B) (Williams et al. 1989). The most negative work is produced at phase 0.65, half of a cycle later. Although these patterns were very consistent across preparations, the total amount of work at any phase varied substantially (see the symbols in Fig. 6B) and was not correlated with the passive properties of that preparation.

The passive muscle and body stress–strain curves are comparable to one another, but isolated muscle has a much more nonlinear response (Fig. 7). Figure 7A and B show example passive work loops. Figure 7C shows passive body and muscle stiffness at low and high strain. The body stiffness does not vary substantially as strain changes, but muscle is much stiffer at high strain. However, the range of the values overlap.

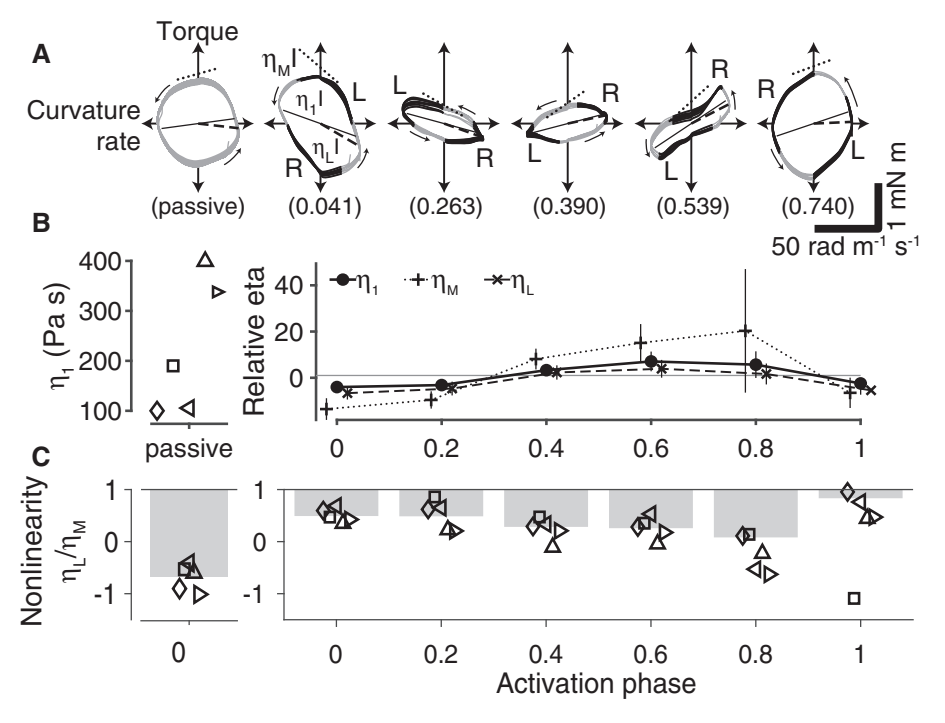


Fig. 5 Effective body damping varies depending on muscle activation phase and is strongly nonlinear. (A) Body torque against curvature rate. Dark lines on the loop indicate the time of muscle stimulation (phase shown in parentheses below each loop), and 'R' and 'L' indicate whether the stimulation is on the right or the left. The three damping moduli are indicated on each curve ( $\eta_1 l$ , the mean overall modulus, solid line;  $\eta_M l$ , the modulus at maximum curvature, dashed line; and  $\eta_L l$ , the modulus at zero curvature, dashed line, displaced upward for clarity). (B) Damping coefficients  $\eta_1$ ,  $\eta_M$ , and  $\eta_L$ , relative to the passive  $\eta_1$  modulus. Error bars are standard deviation and points have been jittered to avoid overlap. (C) Nonlinearity  $\eta_L/\eta_M$ . Means are shown as shaded bars relative to 1, which represents a linear response, and points are individual preparations.

## Local stiffness and damping of isolated muscle segments

To quantify the local stiffness and damping of the muscle segments as a function of length, we used HTFs (Sandberg et al. 2005; Ankarali and Cowan 2014; Kiemel et al. 2016). The local stiffness quantifies the response to a small perturbation at a particular phase in the strain cycle, which is not necessarily the same as the slope of the unperturbed work loop. Figure 8A shows an example of the stress and strain during a perturbed and a baseline trial. Note that there are two phases in these analyses: the strain phase, or the time in the shortening and lengthening cycle; and the activation phase, or the time when the muscle is stimulated. In the above whole-body analysis, we were able to assess the overall stiffness and damping as a function of activation phase; in the isolated muscle analysis, we could quantify both parameters as a function of both phases.

The stress in the muscle depends strongly on the strain phase. This effect can be seen clearly in Fig. 8A; although the strain perturbations are the same at all times, the change in stress is larger when the muscle is

longer. In Fig. 8A, the high stiffness period also corresponds with muscle activation, but this pattern is not always true. The phase dependency is reflected in the Fourier power spectrum (Fig. 8B). For example, one perturbation is at 10.3 Hz, seen as a peak in the gray input trace. In a phase-independent system, this would only cause output at 10.3 Hz, but in the black output trace, several smaller peaks at 8.3 Hz, 9.3 Hz, 11.3 Hz, and 12.3 Hz can be seen on either side of the peak at 10.3 Hz; these are the higher order HTF modes. Note that Fig. 8B has a logarithmic frequency axis, which means that the higher order mode peaks appear closer to the zeroth order peak at higher frequencies.

Based on these data, we computed HTFs, which also show that muscle exhibits phase-dependent stiffness and damping (Fig. 8C). The relatively constant gain at frequencies below 0.8 Hz indicates an elastic response (labeled "stiffness" on Fig. 8C), while the increase in gain at higher frequencies indicates a damping response ("damping" on Fig. 8C). At very high frequencies, however, the gain is lower than would be expected from a simple damper.

Local stiffness increases when the muscles are activated and depends on activation phase (Fig. 9). At

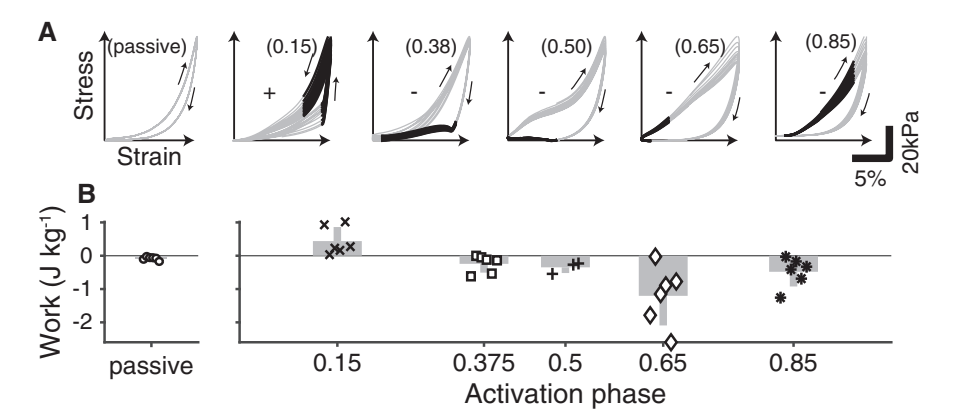


Fig. 6 Muscle work production. (A) Example work loops for isolated muscle at different stimulation phases. Dark lines on the loop indicate the time of muscle stimulation at the phase shown in parentheses. Small arrows show the direction of time in the loop and a '+' or a '-'sign indicates whether the loop shows net positive or net negative mechanical work. (B) Mean mechanical work for five preparations. Each point represents the mean for a single individual, and the bars show the overall mean.

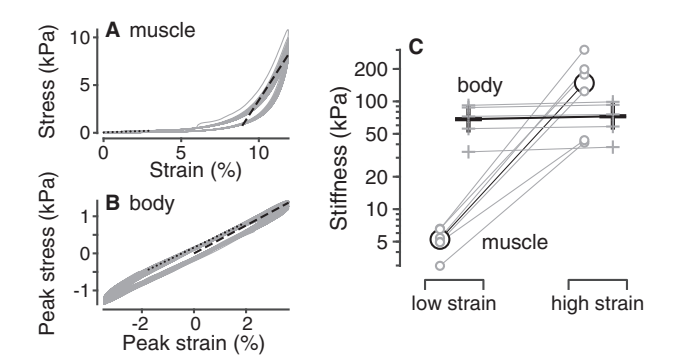


Fig. 7 Passive stiffness measured in the isolated muscle preparation is comparable to the whole body stiffness. Examples of passive work loops for the isolated muscle and whole body are shown in (A) and (B), showing low strain stiffness (dotted line) and high strain stiffness (dashed line). (C) Comparison of stiffness in each preparation. Data from each individual is shown with gray symbols and the overall mean is shown in black.

any phase, stiffness is highest at high strain and in most cases is larger during lengthening than during shortening (Fig. 9A). Average local stiffness is lowest when muscles are generating positive work, and higher at other points in the cycle (Fig. 9B). The ratio of maximum local stiffness and mean local stiffness gives a nonlinearity metric comparable to the one used for the whole-body data. The nonlinearity is  $3.5 \pm 0.6$  in the passive case and  $2.9 \pm 0.7$  in the active case, but does not vary substantially with activation phase.

Local damping shows a similar pattern: it is higher in active muscle and changes with activation phase (Fig. 10). However, the damping is higher when the muscle is producing positive work and lower at other phases (Fig. 10C). Damping nonlinearity is  $13 \pm 9$  in the passive case and  $10 \pm 8$  in the active case, again with no substantial change due to activation phase.

By combining the muscle's HTF with itself shifted by a phase of  $180^{\circ}$ , we were able to mathematically estimate the response of two antagonistic muscles. In this case, the mean stiffness and damping is larger and the variation in maximum stiffness is lower, resulting in a less phase-dependent response, which in our data is a measure of the length-dependent nonlinearity. Nonlinearity in the stiffness of passive and active muscle both decreased by 41% to  $2.1 \pm 0.2$  and  $1.7 \pm 0.2$ , respectively. Nonlinearity in the damping of passive and active muscle decreased by 46% and 42% to  $7.1 \pm 5$  and  $6 \pm 5$ , respectively.

### Discussion

In this study, we demonstrate two techniques for measuring the stiffness and damping of fish bodies. In the first, a whole-body preparation after Long (1998), we quantified stiffness and damping and the large-amplitude nonlinear responses (Porter et al. 2016) of whole fish bodies as they bend from side to side and activate their muscles (Figs. 2 to 5). In the second, a perturbed work loop preparation, we quantified HTFs (Sandberg et al. 2005; Ankarali and Cowan 2014; Kiemel et al. 2016) for isolated muscle segments (Fig. 8). These transfer functions enabled us to predict the response of the muscle to small perturbations at any phase in the strain cycle (Figs. 9 and 10). We found that the stiffness values were in the same range from both techniques. At low strains (<1%) whole body stiffness is higher than muscle stiffness, while at high strains (>5%) muscle is stiffer than the body (Fig. 7C).

The two major results of this work are that (1) muscle stiffness and damping vary depending on phase within the cycle, which is equivalent to muscle length, and (2) these mechanical parameters also

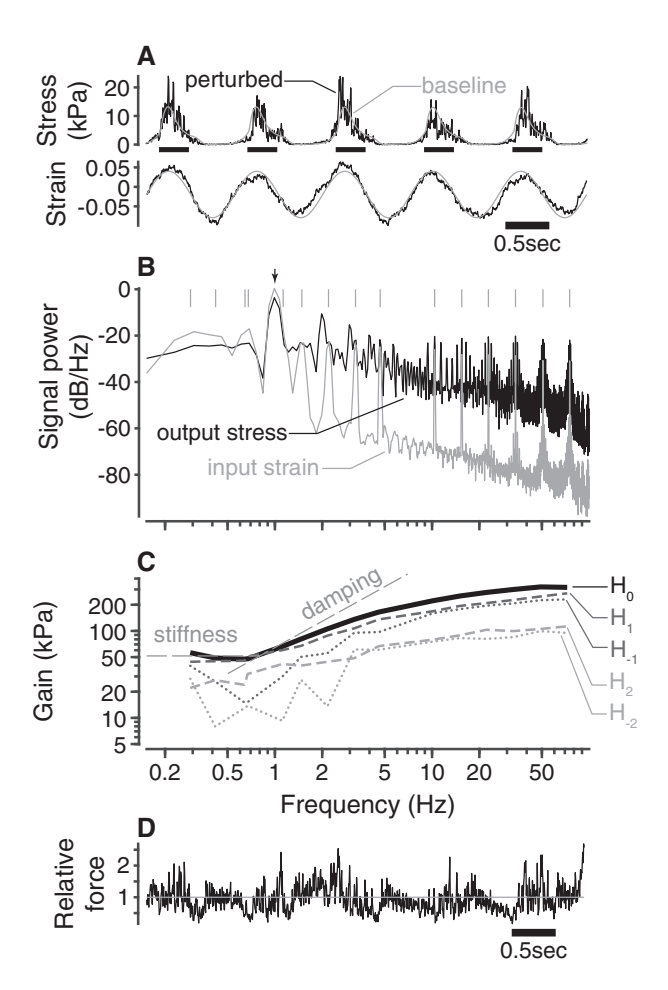


Fig. 8 Example HTF. (A) Raw data, showing the input muscle strain and output stress, with the baseline and perturbed trials shown in gray and black, respectively. Black bars indicate when the muscle was stimulated. (B) Spectral power density plots for the input stress and output stress in gray and black, respectively. The fundamental frequency is shown with a black arrow, and perturbation frequencies are shown with gray ticks. (C) Gain of the HTF. Higher order modes are shown in lighter grays, and positive and negative modes are shown with dashed and dotted lines, respectively. A purely elastic response would have a constant gain, indicated by the dashed line labeled "stiffness" and a purely damping response would increase proportional to frequency, indicated by the dashed line labeled "damping". (D) Perturbed force as a fraction of the baseline.

change substantially depending on the phase of activation.

# Isolated muscle has phase-dependent stiffness and damping

Muscle can be approximated as having a stiffness and damping that depend on the phase within the shortening and lengthening cycle. A system with linear elasticity and damping would have a constant gain relative to frequency at low frequencies and a gain that increases proportional to frequency at high

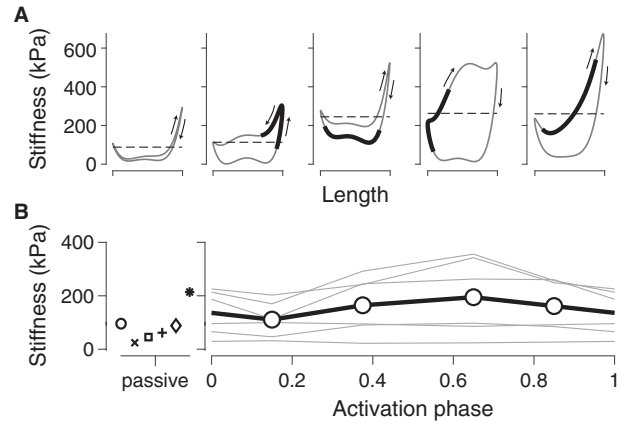


Fig. 9 Length-dependent stiffness of isolated muscle. (A) Example plots of stiffness against length for one individual. Thick lines show when the muscle is stimulated and dashed lines indicate the mean stiffness. (B) Overall mean stiffness as a function of activation phase. Gray lines show individual data and thick black lines show the overall mean.

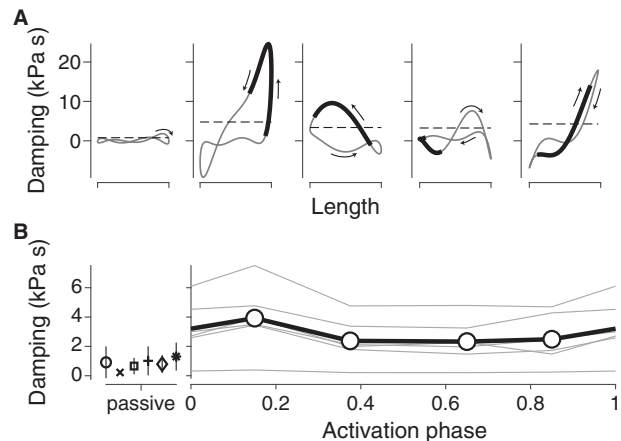


Fig. 10 Length-dependent damping of isolated muscle. (A) Example plots of damping against length for one individual. Thick lines show when the muscle is stimulated and dashed lines indicate the mean stiffness. (B) Overall mean damping as a function of activation phase. Gray lines show individual data and thick black lines show the overall mean.

frequencies. This is the pattern we observe in the zeroth-order HTF and higher order modes (Fig. 8C), indicating a phase-dependent stiffness and damping. The response magnitude rolls off at high frequencies, a decline that is characteristic of inertial effects, although inertia is not usually thought to contribute to the dynamics of muscle contraction (e.g., Telley et al. 2006).

To our knowledge, no one has estimated the phase-dependent properties of muscle in this way before, but some have used similar techniques to examine the phase-independent properties. Palmer et al (2007) and Tanner et al. (2011) used sinusoidal oscillations and white noise perturbations,

respectively, to examine the phase-independent mechanical properties of cardiac muscle from mice. They found a similar relationship: the stiffness in relatively constant at frequencies below 10 Hz and then rises, but falls off at high frequencies (Palmer et al. 2007; Tanner et al. 2011). Ettema and Huijing (1994b), in contrast, found that the stiffness of active rat gastrocnemius muscles was relatively constant at low frequencies, declined at intermediate frequencies, and increased again at higher frequencies. None of these studies quantified damping coefficients.

### Muscle stiffness is strongly nonlinear

Muscle has a very low stiffness at low strain and a much higher stiffness at high strain. This effect can be seen clearly in Fig. 8A, in which the perturbations are of the same size at all strains, but the change in stress is much higher at high strain. This finding is consistent with many other previous studies of muscle, which have characterized the passive stiffness as an exponential spring (Glantz 1974; Brown et al. 1996; Lappin et al. 2006; Monroy et al. 2017). If muscle force increases exponentially with strain, then we can remove the effect of strain by dividing by the baseline force, because stiffness depends on force (Ettema and Huijing 1994a). Indeed, in Fig. 8D, we see that the relative force for a perturbed trial divided by its baseline does not vary consistently over time.

In the HTFs, the length dependence of muscle stiffness can be seen as a phase dependence, because length and force change with phase. The  $H_{\pm 1}$  modes have gains that are comparable to the gain of  $H_0$ , which shows a phase dependent response (Fig. 8C).

The local stiffness that we measured is different from short-range stiffness (Campbell 2010). Short-range stiffness is an effect that results from stretching myosin cross-bridges over very short lengths, and can be observed at the very beginning of a lengthening perturbation (Campbell 2010). Because our approach is phase-dependent, it should account for the activation-dependent change in short-range stiffness (Campbell and Moss 2002), but our perturbations are larger than those typically used to examine the short-range stiffness effects.

Nishikawa et al. (2012), Herzog (2014) and Powers et al. (2017) have recently been developing the "winding-filament" model of muscle, in which the muscle stiffness due to the titin molecule increases when the muscle produces force. This model can account for force enhancement after active stretch, in which muscle produces extra force after a short stretch (Herzog and Leonard 2002). Our approach also shows that muscle has a higher

local stiffness during active lengthening. The HTF approach also has the potential to address the long-lasting force enhancement that occurs after the stretch is completed. To estimate force enhancement, we would need to compute a phase-dependent impulse response function, the equivalent of an inverse Fourier transform for an HTF, which describes the time course of the response due to a small perturbation at any phase (Kiemel et al. 2016). However, to estimate the impulse response function accurately, the HTF must become small at high frequencies (Kiemel et al. 2016), which is not true for our data (Fig. 8C). In further work, higher frequencies will be examined in order to estimate the phase-dependent impulse response.

### Lamprey bodies are extremely flexible, but can change their effective stiffness and damping

Lamprey bodies are extremely flexible, with an average passive stiffness of  $73 \pm 26$  kPa. For comparison, this is about the same as one of the most flexible artificial elastomers available for purchase (Ecoflex 00-10), which has a stiffness of 55 kPa. There are few measurements from other species with which to compare, but Long and colleagues have measured stiffness of ~390 kPa for eels (Long 1998) and 240 kPa for hagfishes (Long et al. 2002), based on their published figures. Our measured stiffness is much lower even than what they found for the hagfish, a related and very flexible species. The difference may be because the bending amplitudes used here (±5 rad m<sup>-1</sup>), even though they are characteristic of swimming adult lampreys (Hultmark et al. 2007), are substantially lower than those used by Long (2002).

Effective body stiffness can change depending on activation, increasing to as much as  $160 \pm 30\%$  over passive at a muscle activation phase of 0.76 and decreasing to  $45 \pm 30\%$  of passive at an activation phase of 0.38 (Fig. 5). This is a similar, but slightly smaller, range than what Long (1998) found for eels, where stiffness reached a maximum of 235% of passive at a phase of 0.85 and a minimum of 35% at phase 0.35.

The mean passive body damping  $\eta_1$  of lampreys is also quite low,  $0.22 \pm 0.13 \, \text{kPa}$  s at a frequency of 1 Hz. In the passive case, the minimum strain damping  $\eta_M$  is higher, up to  $0.63 \, \text{kPa}$  s for the most damped individual. However, based on Long's measurements, eels have a passive damping that is about 50 times higher, 11 kPa s, at 3 Hz, and hagfish have a damping of about 5.7 kPa s at 1 Hz. Hagfish had lower damping at higher frequencies, dropping to

about  $2 \,\mathrm{kPa}$  s at  $3 \,\mathrm{Hz}$ . It is possible that the differences in these estimates is related to the different methods for estimating the parameters. We used the large amplitude bending method developed by Ewoldt (Ewoldt et al. 2008; Porter et al. 2016), while Long used classic linear bending mechanics (Den Hartog 1985; Long 1998). However, Porter et al (2016) estimated the damping of the vertebral columns of sharks using the same method, and found that  $\eta_1$  was about 22 kPa s at 1 Hz and curvature of 5 rad m<sup>-1</sup>. In our analysis, the damping measurements were consistently low across the five individuals; further tests will be needed to determine if this very low damping is a characteristic of lampreys.

Damping changes dramatically as muscle activation changes. We also find consistent negative damping at some phases. Long (1998) found both of these effects in eels, with damping increasing or decreasing between about  $\pm 5$  times the passive damping, and the largest damping occurring at a phase of 0.4. Negative damping may indicate that the muscle is aiding the movement, so that the torque required becomes lower as the velocity increases, but it can also happen at high curvature rates in passive tissues.

### Whole-body body stiffness is linear

Although lampreys can alter their effective body stiffness depending on muscle activation, the body stiffness at a particular activation phase behaves mostly linearly with respect to curvature, with roughly the same stiffness at low and high curvature (Fig. 4D). Unlike stiffness, damping was highly nonlinear, with substantially different minimum strain and large strain damping. On average, damping is about 40% lower at high curvature rates, which is similar to that in hagfish (Long et al. 2002).

# Antagonistic muscles decrease nonlinearity

The linearity of the whole-body response may seem somewhat surprising, given that the muscles are so nonlinear, particularly in their passive state. One explanation is that the strains in the whole-body preparation were quite low, and muscle nonlinearities are particularly strong at high strain. However, multiple factors may be important in decreasing the overall nonlinearity.

The body has a complex internal structure (Vogel and Gemballa 2001; Danos et al. 2008). It might seem that this complex structure would lead to a nonlinear response. However, strain in the muscle can be predicted accurately by assuming that the body is a homogenous elastic beam (Coughlin

et al. 1996; Long et al. 2002). This suggests that this complex morphology helps to increase the linearity of the response (Long et al. 2002).

Here, we also showed that, in the active state, antagonistic muscles may help to cancel out some of the nonlinearities of their individual responses. Specifically, pairs of antagonist muscles respond in a less phasedependent way than either one individually. Mathematically, this result comes from the way HTFs combine with one another. Shifting phase by 180° means flipping the sign of the odd modes of the transfer functions  $(H_{\pm 1}, H_{\pm 3}, \ldots)$ . Combining this with the original transfer function means that the even modes double and the odd modes go to zero. In our data, the average magnitude of higher order modes decreases as the order of the mode increases (Fig. 9C), such that the modes with the largest gain at most frequencies are  $H_0$  and  $H_{\pm 1}$ . For an antagonistic pair of muscles, the large nonlinear effects of  $H_{\pm 1}$  cancel each other out, leaving the linear behavior of  $2H_0$  and some relatively smaller nonlinear effects from  $2H_{\pm 2}$ ,  $2H_{\pm 4}$ , and higher-order even modes. In contrast, if the modes with the largest gain were  $H_0$ and  $H_{\pm 2}$ , one would expect only a minor reduction in nonlinearity for a pair of antagonistic muscles, but this case corresponds to stiffness having two peaks within the strain cycle, which is not consistent with our results or previous (Ettema and Huijing 1994a; Monroy et al. 2017). Therefore, we suggest that antagonistic pairs of muscles are always less phase-dependent than single muscles. In our analysis, the phase dependence seems to result from a nonlinear stiffness that changes with length or force. Therefore, if phase dependence is reduced in antagonistic muscle pairs, the overall nonlinearity of the system is also reduced.

### Implications for motor control

Using a computational model, we previously showed that stiffer fish with higher muscle forces accelerate faster than more flexible fish with lower muscle forces, but that the more flexible fish use less energy when swimming steadily (Miller et al. 2012). We suggested that fish might increase their effective stiffness in order to accelerate more rapidly. By activating muscle before the beginning of shortening, the effective body stiffness increases, even as the muscle continues to produce positive mechanical work (compare phase 0.25 and 0 in Fig. 4). Indeed, Johnson et al. (1994) found that largemouth bass *Micropterus salmoides* activate their muscles earlier in the tailbeat cycle during burst and glide swimming.

Activating muscles near a phase of zero may also help acceleration performance because of the change in damping. At a phase of zero, effective stiffness is high but damping is low and negative (Fig. 5). This means that the body will tend to aid rapid body movements, because damping decreases as speed increases. Finally, when activated at this phase, the local stiffness and damping of muscle is high, which may help to reject perturbations.

### **Data**

All data and processing algorithms from this study are available online at doi: 10.6070/H4765CX7.

### **Acknowledgments**

We thank Kiisa Nishikawa for helpful discussions of the ideas in this paper.

### **Funding**

This material is based upon work supported by the Army Research Office under grant number W911NF-14-1-0268 (to EDT), the National Science Foundation under Grant No. IOS-1230311 and IOS-1230493 (to TK and NJC), and by the Scientific Research Projects Coordination Unit of METU under Project no. YÖP-301-2018-2842 (to MMA). Support for participation in this symposium was provided by Photron (https://photron.com), the Company of Biologists, the Society for Integrative Comparative Biology (Divisions Comparative Biomechanics, Vertebrate Morphology, Animal Behavior, and NNSB), the Air Force Office of Scientific Research (FA9550-16-1-0165), and the National Science Foundation (IOS-1747859).

### References

- Ahn AN, Full RJ. 2002. A motor and a brake: two leg extensor muscles acting at the same joint manage energy differently in a running insect. J Exp Biol 205:379–89.
- Ankarali MM, Cowan NJ. 2014. System identification of rhythmic hybrid dynamical systems via discrete time harmonic transfer functions. In: IEEE Annual Conference on Decision and Control (doi: 10.1109/CDC.2014.7039515).
- Azizi E, Roberts TJ. 2009. Biaxial strain and variable stiffness in aponeuroses. J Physiol 587:4309–18.
- Brown IE, Loeb GE. 2000. A reductionist approach to creating and using neuromusculoskeletal models. In: Winters JM, Crago P, editors. Biomechanics and neuro-control of posture and movement. New York: Springer-Verlag. p. 148–63.
- Brown IE, Scott SH, Loeb GE. 1996. Mechanics of feline soleus: iI Design and validation of a mathematical model. J Muscle Res Cell Motil 17:221–33.
- Cameron BA, Tufts BL. 1994. *In vitro* investigation of the factors contributing to the unique CO<sub>2</sub> transport properties of blood in the sea lamprey (*Petromyzon marinus*). J Exp Biol197:337–48.

- Campbell KS. 2010. Short-range mechanical properties of skeletal and cardiac muscles. In: Rassier DE, editor. Muscle biophysics: from molecules to cells New York: Springer. p. 223–46.
- Campbell KS, Moss RL. 2002. History-dependent mechanical properties of permeabilized rat soleus muscle fibers. Biophys J 82:929–43.
- Coughlin DJ, Valdes L, Rome LC. 1996. Muscle length changes during swimming in scup: sonomicrometry verifies the anatomical high-speed cine technique. J Exp Biol 199:459–63.
- Danos N, Azizi E. 2015. Passive stiffness of hindlimb muscles in anurans with distinct locomotor specializations. Zoology 118:239–47.
- Danos N, Fisch N, Gemballa S. 2008. The musculotendinous system of an anguilliform swimmer: muscles, myosepta, dermis, and their interconnections in *Anguilla rostrata*. J Morphol 269:29–44.
- Dauble DD, Moursund RA, Bleich MD. 2006. Swimming behaviour of juvenile Pacific lamprey, *Lampetra tridentata*. Environ Biol Fishes75:167–71.
- Den Hartog JP. 1985. Mechanical vibrations. 4th ed. New York: Dover Publications.
- Ettema GJC, Huijing PA. 1994a. Skeletal muscle stiffness in static and dynamic contractions. J Biomech 27:1361–8.
- Ettema GJC, Huijing PA. 1994b. Frequency response of rat gastrocnemius medialis in small amplitude vibrations. J Biomech 27:1015–22.
- Ewoldt RH, Hosoi AE, McKinley GH. 2008. New measures for characterizing nonlinear viscoelasticity in large amplitude oscillatory shear. J Rheol 52:1427–58.
- Forssberg H, Grillner S, Rossignol S. 1975. Phase dependent reflex reversal during walking in chronic spinal cats. Brain Res 85:103–7.
- Glantz SA. 1974. A constitutive equation for the passive properties of muscle. J Biomech 7:137–45.
- Grillner S. 2003. The motor infrastructure: from ion channels to neuronal networks. Nat Rev Neurosci 4:573–86.
- Grillner S, Wallén P, Brodin L, Lansner A. 1991. Neuronal network generating locomotor behavior in lamprey circuitry, transmitters, membrane-properties, and simulation. Annu Rev Neurosci 14:169–99.
- Grillner S, Williams TL, Lagerbäck P-Å. 1984. The edge cell, a possible intraspinal mechanoreceptor. Science 223:500–3.
- Herzog W. 2014. Mechanisms of enhanced force production in lengthening (eccentric) muscle contractions. J Appl Physiol 116:1407–17.
- Herzog W, Leonard TR. 2002. Force enhancement following stretching of skeletal muscle: a new mechanism. J Exp Biol 1283:1275–83.
- Holmes PJ, Full RJ, Koditschek DE, Guckenheimer JM. 2006. The dynamics of legged locomotion: models, analyses, and challenges. SIAM Rev 48:207–304.
- Hultmark M, Leftwich MC, Smits AJ. 2007. Flowfield measurements in the wake of a robotic lamprey. Exp Fluids 43:683–90. Jindrich DL, Full RJ. 2002. Dynamic stabilization of rapid hexapedal locomotion. J Exp Biol 205:2803–23.
- Johnson TP, Syme DA, Jayne BC, Lauder GV, Bennett AF. 1994. Modeling red muscle power output during steady and unsteady swimming in largemouth bass. Am J Physiol 267:R481–8.

Kiemel T, Logan D, Jeka JJ. 2016. Using perturbations to probe the neural control of rhythmic movements. arXiv:1607.01746.

- Kimura T, Watanabe T, Egawa K, Takiguchi R. 1995. Architecture and muscle fiber types of lamprey myotome. Biomed Res 16:21–31.
- Lacey RW, Neary VS, Liao JC, Enders EC, Tritico HM. 2012. The IPOS framework: linking fish swimming performance in altered flows from laboratory experiments to rivers. River Res Appl 28:429–43.
- Lappin AK, Monroy JA, Pilarski JQ, Zepnewski ED, Pierotti DJ, Nishikawa KC. 2006. Storage and recovery of elastic potential energy powers ballistic prey capture in toads. J Exp Biol 209:2535–53.
- Lin DC, Rymer WZ. 2000. Damping actions of the neuromuscular system with inertial loads: soleus muscle of the decerebrate cat. J Neurophysiol 83:652–8.
- Long JH. 1998. Muscles, elastic energy, and the dynamics of body stiffness in swimming eels. Am Zool 38:771–92.
- Long JH, Adcock B, Root RG. 2002. Force transmission via axial tendons in undulating fish: a dynamic analysis. Comp Biochem Physiol A 133:911–29.
- Long JH, Koob-Emunds M, Sinwell B, Koob TJ. 2002. The notochord of hagfish *Myxine glutinosa*: visco-elastic properties and mechanical functions during steady swimming. J Exp Biol 205:3819–31.
- Massarelli N, Yau A, Hoffman K, Kiemel T, Tytell ED. 2016. Understanding locomotor rhythm in the lamprey central pattern generator. In: Letzter G, Lauter K, Chambers E, Flournoy N, Grigsby JE, Martin C, Ryan K, Trivisa K, editors. Advances in the mathematical sciences. Switzerland: Springer International Publishing. p. 157–72.
- Massarelli N, Yau AL, Hoffman KA, Kiemel T, Tytell ED. 2017. Characterization of the encoding properties of intraspinal mechanosensory neurons in the lamprey. J Comp Physiol A 203:831–41.
- Mesa MG, Bayer JM, Seelye JG. 2003. Swimming performance and physiological responses to exhaustive exercise in radiotagged and untagged Pacific lampreys. Trans Am Fish Soc 132:483–92.
- Miller LA, Goldman DI, Hedrick TL, Tytell ED, Wang ZJ, Yen J, Alben S. 2012. Using computational and mechanical models to study animal locomotion. Integr Comp Biol 52:553–75.
- Monroy JA, Powers KL, Pace CM, Uyeno T, Nishikawa KC. 2017. Effects of activation on the elastic properties of intact soleus muscles with a deletion in titin. J Exp Biol 220:828–36.
- Nishikawa KC, Monroy JA, Uyeno TE, Yeo SH, Pai DK, Lindstedt SL. 2012. Is titin a 'winding filament'? A new twist on muscle contraction. Proc R Soc Lond B 279:981–90.
- Ogata K. 2010. Modern control engineering. 5th ed. Boston: Prentice-Hall.
- Palmer BM, Suzuki T, Wang Y, Barnes WD, Miller MS, Maughan DW. 2007. Two-state model of acto-myosin attachment-detachment predicts C-process of sinusoidal analysis. Biophys J 93:760–9.
- Parker D. 2006. Complexities and uncertainties of neuronal network function. Philos Trans R Soc Lond B 361:81–99.

Peplowski MM, Marsh RL. 1997. Work and power output in the hindlimb muscles of Cuban tree frogs *Osteopilus septentrionalis* during jumping, J Exp Biol200:2861–70.

- Porter ME, Ewoldt RH, Long JH. 2016. Automatic control: the vertebral column of dogfish sharks behaves as a continuously variable transmission with smoothly shifting functions. J Exp Biol 219:2908–19.
- Powers KL, Joumaa V, Jinha A, Moo EK, Smith IC, Nishikawa K, Herzog W. 2017. Titin force enhancement following active stretch of skinned skeletal muscle fibres. J Exp Biol (doi: 10.1242/jeb.153502).
- Proctor J, Holmes P. 2010. Reflexes and preflexes: on the role of sensory feedback on rhythmic patterns in insect locomotion. Biol Cybern 102:513–31.
- Quintella BR, Andrade NO, Koed A, Almeida PR. 2004. Behavioural patterns of sea lampreys' spawning migration through difficult passage areas, studied by electromyogram telemetry. J Fish Biol 65:961–72.
- Rossignol S, Dubuc RJ, Gossard J-P. 2006. Dynamic sensorimotor interactions in locomotion. Physiol Rev 86:89–154.
- Roth E, Sponberg S, Cowan NJ. 2014. A comparative approach to closed-loop computation. Curr Opin Neurobiol 25:54–62
- Sandberg H, Möllerstedt E, Bernhardsson B. 2005. Frequency-domain analysis of linear time-periodic systems. IEEE Trans Autom Control 50:1971–83.
- Sponberg S, Libby T, Mullens CH, Full RJ. 2011. Shifts in a single muscle's control potential of body dynamics are determined by mechanical feedback. Philos Trans R Soc Lond B 366:1606–20.
- Summers AP, Long JH. 2005. Skin and bones, sinew and gristle: the mechanical behavior of fish skeletal tissues. In: Shadwick RE, Lauder GV, editors. Fish physiology. Amsterdam: Elsevier. p. 141–77.
- Tanner BCW, Wang Y, Maughan DW, Palmer BM. 2011. Measuring myosin cross-bridge attachment time in activated muscle fibers using stochastic vs. sinusoidal length perturbation analysis. J Appl Physiol 110:1101–8.
- Telley IA, Denoth J, Stüssi E, Pfitzer G, Stehle R. 2006. Half-sarcomere dynamics in myofibrils during activation and relaxation studied by tracking fluorescent markers. Biophys J 90:514–30.
- Teräväinen H. 1971. Anatomical and physiological studies on muscles of lamprey. J Neurophysiol 34:954–73.
- Tytell ED, Cohen AH. 2008. Rostral versus caudal differences in mechanical entrainment of the lamprey central pattern generator for locomotion. J Neurophysiol 99:2408–19.
- Tytell ED, Holmes P, Cohen AH. 2011. Spikes alone do not behavior make: why neuroscience needs biomechanics. Curr Opin Neurobiol 21:816–22.
- Vogel F, Gemballa S. 2001. Locomotory design of "cyclostome" fishes: spatial arrangement and architecture of myosepta and lamellae. Acta Zool 81:267–83.
- Wereley NM. 1991. Analysis and control of linear periodically time varying systems [Ph.D. dissertation]. [Dept. Aeronautics and Astronautics, Mass. Inst. Tech].
- Williams TL, Grillner S, Smoljaninov VV, Wallén P, Kashin S, Rossignol S. 1989. Locomotion in lamprey and trout: the relative timing of activation and movement. J Exp Biol 143:559–66.